DMI
Ministry of Transport and Energy

Scientific Report 06-05

Simulation of the seasonal sea ice microwave emissivity variability

A demonstration of model functionality

Rasmus T. Tonboe

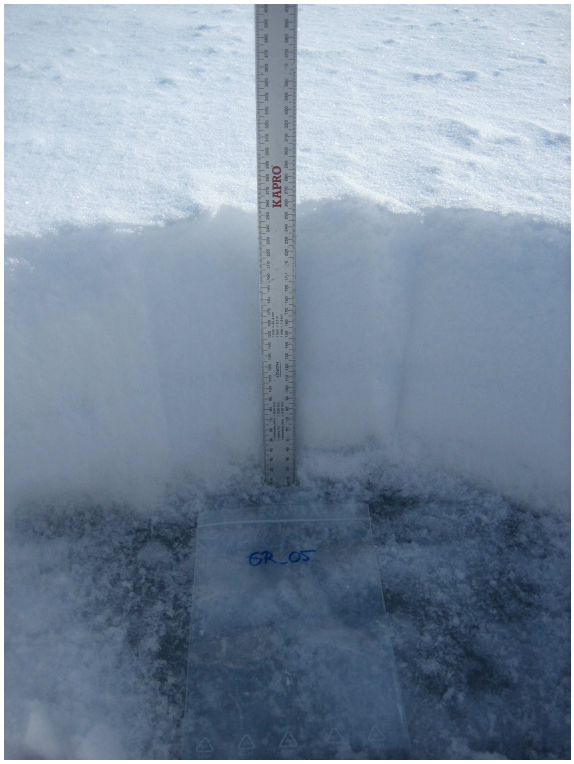

Snow profile on first-year ice in the Arctic Ocean, North of Alert. Photo S. Hanson.

Copenhagen 2006

Colophon

Serial title:
Scientific Report 06-05

Title:
Simulation of the seasonal sea ice microwave emissivity variability

Subtitle:
A demonstration of model functionality

Author(s):
Rasmus T. Tonboe

Other contributors:

Responsible institution:
Danish Meteorological Institute

Language:
English

Keywords:

Url:
www.dmi.dk/dmi/sr06-05

Digital ISBN:
87-7478-539-7

ISSN:
1399-1949

Version:
September 2006

Website:
www.dmi.dk

Content:

Abstract 4
Resumé 4
INTRODUCTION 5
MICROWAVE ATMOSPHERIC SOUNDING IN THE SEMITRANSPARENT ATMOSPHERE 5
BAGGROUND: SEA ICE SURFACE EMISSIVITY MEASUREMENTS 5
SEASONAL VARIABILITY OF THE SNOW COVER 6
SIMPLE PARAMETERISATION OF THE EMISSIVITY AND EFFECTIVE TEMPERATURE 9
MEAN SEASONAL MICROWAVE PARAMETERS 11
DISCUSSION OF SEASONAL EMISSIVITY VARIATIONS 12
REFERENCES 12
APPENDIX 13
Previous reports 14

Abstract

A sea ice version of MEMLS (Wiesmann & Mätzler, 1999) is used to study the sea ice microwave emissivity. Output from a thermodynamic model using ECMWF re-analysis data is input to the emissivity model to simulate the seasonal variability in the Arctic Ocean. This ongoing work is part of the EU 6th framework programme project DAMOCLES.

Resumé

En havisversion af MEMLS (Wiesmann & Mätzler, 1999) er brugt til at undersøge mikrobølgee-missiviteten fra havis. Outputtet fra en termodynamisk model der bruger ECWMF reanalyse data anvendes som input til emissivitetsmodellen for at simulere variabiliteten i løbet af vinteren i det Arktiske Ocean. Dette arbejde fortsættes i EU's 6te rammeprogram projekt DAMOCLES.

INTRODUCTION

The microwave brightness temperature of a lossy half-space (snow/ sea ice) is the product of the thermometric temperature and the emissivity. The emissivity, at a certain polarisation, frequency and angle, is a function of subsurface extinction and reflections between layers with different permittivity. The microwave penetration depth in snow (>100GHz) is in the order of centimetres due to significant extinction. Models relate physical snow and ice properties such as density, temperature, snow crystal and brine inclusion size to microwave attenuation, scattering and reflectivity. The model used here is a sea ice version of MEMLS (Wiesmann & Mätzler, 1999) described in Mätzler et al. (2006) and hereafter called the emission model. The emission model is used to simulate the sea ice brightness temperature (Tb), emissivity (e) and effective thermometric temperature (T_{eff}) variability as a function of a seasonal snow and ice cover. Output from a mass and thermodynamic sea ice model (Tonboe, 2005) is used to assess the seasonal variability of these parameters in the central Arctic Ocean. This model is hereafter called the thermodynamic model. The aim with our model experiments is to start understanding the microwave emission from sea ice in applications such as for assimilation, i.e. atmospheric sounding, in numerical weather prediction models. Further, to demonstrate the model functionality.

MICROWAVE ATMOSPHERIC SOUNDING IN THE SEMITRANSPARENT ATMOSPHERE

The Arctic sea ice cover 3% and the Antarctic sea ice cover 4% of Earth's surface in their respective winters. At any time, about 4-5% of Earth's surface is covered by sea ice. Open ocean microwave brightness temperatures measured by satellite radiometers at sounding frequencies e.g. 23, 50, 150 and 183GHz from the AMSU A/B instruments on the polar orbiting NOAA satellites are assimilated into NWP models. The measurements are prominent for information on atmospheric temperature and humidity and have a significant positive impact on NWP model forecast skill. The use of these data for atmospheric sounding is possible because of models describing the *open* ocean surface emissivity at these frequencies. Such models does not exist for snow and ice emissivity and satellite microwave sounding measurements are not assimilated in Arctic snow and sea ice covered regions where the atmosphere is most often semitransparent even at these frequencies (Data are assimilated whenever the atmosphere is opaque). Conventional meteorological measurements, such as meteorological stations and radiosondes, are sparse in Arctic regions. Atmospheric conditions in the Arctic nevertheless influence the weather in Denmark and other regions at these relatively high latitudes. New results (the EU project IOMASA, 2002-2005) indicate that the scarcity of suitable assimilation data in the Arctic gives systematic biases in NWP model fields (air temperature) and that forecast skill even over Europe is degraded. The development of reliable emissivity models for snow and ice would have an immediate impact on weather forecasting not only in the regions where the Danish Meteorological Institute (DMI) is responsible (Denmark, Faeroe Islands and Greenland) but also globally, not least the Southern Ocean and Antarctica where meteorological measurements are particularly sparse. Satellite coverage in Polar Regions is dense and if just 5% of these data could be exploited this would be considered a break-through.

BAGGROUND: SEA ICE SURFACE EMISSIVITY MEASUREMENTS

Both the surface brightness temperature and effective temperature are needed to derive microwave emissivity. Since snow/ice temperature profiles are not available on spatial scales covered by airborne microwave radiometers, the skin temperature, which can be measured by infrared radiometers, is often used instead (Hewison & English, 1999; Haggerty & Curry, 2001). The error is small during spring and summer when the snow/ice is relatively isothermal and/or the penetration is

limited. During winter when the surface is most often colder than the snow/ice interior the emissivity is overestimated (most points are above the diagonal in figure 13). Relatively few campaigns have focussed on sea ice and microwave frequencies above 90GHz (e.g. Hewison & English, 1999; Haggerty & Curry, 2001). Nadir emissivities from these campaigns are summarised in Tab. 1.

Type	Nadir emissivity				Reference
	24GHz	**50GHz**	**89GHz**	**157GHz**	
Baltic fast ice (April)	0.872	0.744	0.672	0.696	Hewison & English, 1999
Baltic bare new ice (April)	0.923	0.918	0.910	0.915	Hewison & English, 1999
	37GHz	**90GHz**	**150GHz**	**220GHz**	
Arctic (May)	0.89	0.73	0.72	0.84	Haggery & Curry, 2001

Table 1 Summary of nadir emissivity for different ice types.

SEASONAL VARIABILITY OF THE SNOW COVER

Figure 1-8 show the simulated snow surface density on first- and multiyear ice at two positions in the central Arctic Ocean during the 2000/2001 winter season using ECMWF re-analysis data as input to the thermodynamic model (82.5ºN; 0.0ºE between Fram Strait and the North Pole and 82.5ºN; 180.0ºE between the North Pole and the Bering Strait). Precipitation events less than 1kg/m^2 (snow water equivalent < 1mm) are not included. The simulations begin with a bare ice surface on Sep. 1., which is approximately the end of the melt season. The multiyear ice simulation begin with an 3.5m ice profile which gradually grows to more than 5m and the first-year ice profile grows from 0.1m to over 2m. The emission model is coupled to the thermodynamic model and the seasonal variability of microwave parameters is computed. All simulations are at 50º incidence angle. The melt processes during the summer season are complicated and not sufficiently described by the thermodynamic model. Summer melt is therefore not included in this study.

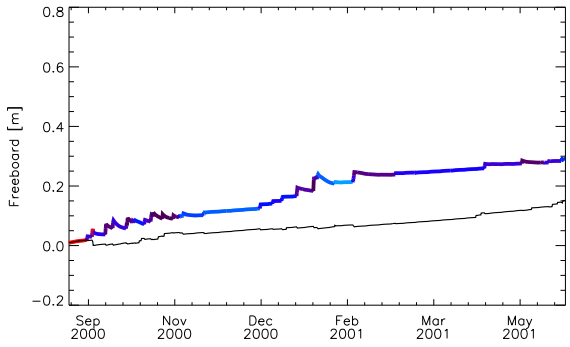

Figure 1 first-year ice 82.5N 0.0E

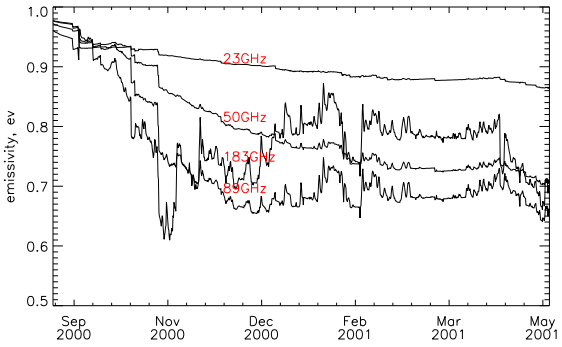

Figure 2 first-year ice at 82.5N, 0.0E

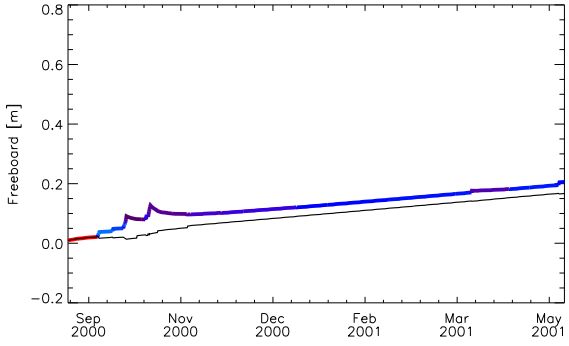

Figure 3 first-year ice 82.5N, 180.0E

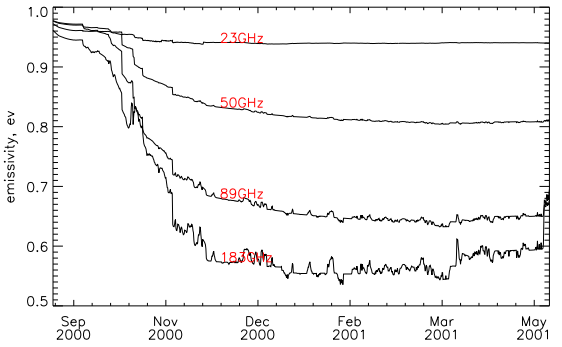

Figure 4 first-year ice at 82.5N, 180.0E

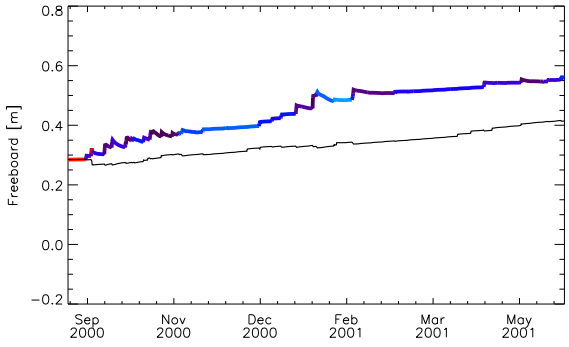

Figure 5 Multiyear ice 82.5N, 0.0E

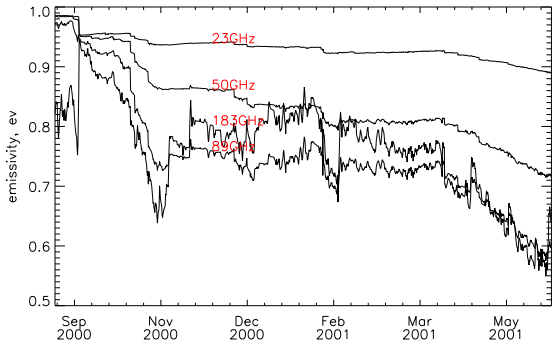

Figure 6 Multiyear ice at 82.5N, 0.0E

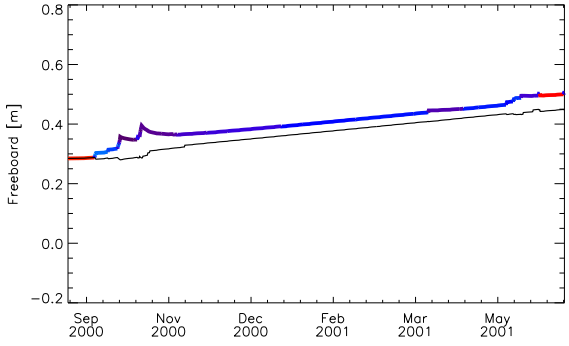

Figure 7 Multiyear ice 82.5N, 180.0E

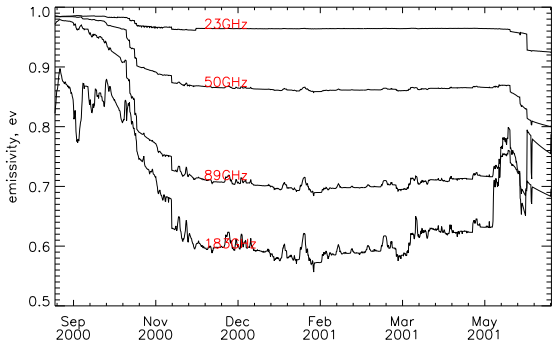

Figure 8 Multiyear ice at 82.5N, 180.0E

The level of emissivities shown for the four profiles above is within the limits outlined in Tab. 1. For the thin snow profiles at 82.5N, 180.0E there is a gradient with decreasing emissivity for increasing frequency during winter. The two profiles where the snow cover is relatively thick (82.5N, 0.0E) the 183GHz emissivity is generally higher than the 89GHz emissivity during winter. The largest variations occur during freeze-up and melt as expected. The multiyear ice emissivity at 82.5N, 0.0E (fig. 6) decrease from March to May due to the accelerated metamorphosis of the snow cover, in particular with snow grain size growth. The average snow pack correlation length, a measure of snow grain size, is shown vs. the 50GHz emissivity in figure 9.

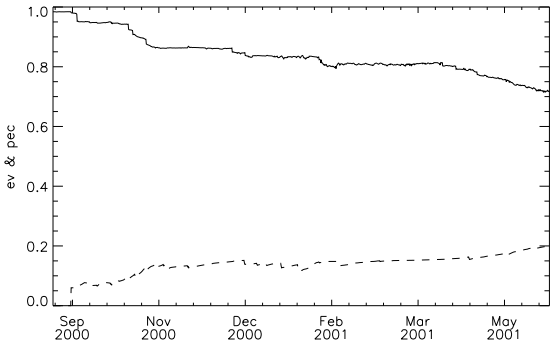

Figure 9 The multiyear ice emissivity at 50GHz (82.5N, 0.0E) solid line and the average snow correlation length (measure of snow grain size) dashed line. The correlation coefficient is -0.95.

SIMPLE PARAMETERISATION OF THE EMISSIVITY AND EFFECTIVE TEMPERATURE

Recent experiments in the EU-IOMASA project (2002-2005) by Schyberg and others (not published – yet) show that AMSU A surface emissivity (e.g. 50GHz) can be estimated from emissivity tie-points in a linear combination of first and multiyear ice concentrations. We therefore investigate the possibilities relating the emissivity and effective temperature to simple and measurable parameters. Figure 10 shows the emissivity at 50GHz vs. the spectral gradient at 19 and 37 GHz, $GR_{19/37}$ using all data.

$$GR_{19/37} = \frac{Tb_{37V} - Tb_{19V}}{Tb_{37V} + Tb_{19V}} \qquad \text{eq. 1.}$$

$GR_{19/37}$ is in fact used for determining the first and multiyear ice concentrations in Schybergs experiment and we see the relationship. The figure (10) also shows that the emissivity is not actually related to the ice type but rather the scattering properties of the snow cover. Other such relationships between the spectral gradient and the emissivity were tested but these were not as clear.

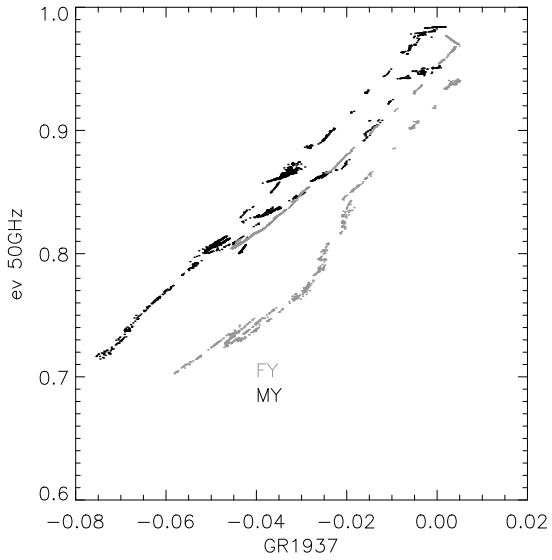

Figure 10 The spectral gradient ($GR_{19/37}$) vs. the 50GHz emissivity. The two first-year ice profiles are shown with grey points and the two multiyear ice profiles are shown with black

points.

The brightness temperature, Tb, is the product of the emissivity, e, and the integrated emitting layer physical temperature or the effective temperature, T_{eff}, i.e. $Tb=e*T_{eff}$. Even at high frequency 150 and 183GHz shown in figure 11 and 12 there can be significant differences between the air temperature, Ta, and the effective temperature. There are no clear relationships at lower frequencies because of deeper penetration. It was further noted by Haggerty & Curry (2001) that the surface skin temperature, not necessarily synonymous with the air temperature, is only a good proxy for the effective temperature during relatively isothermal conditions in spring and early summer. The skin temperature vs. the effective temperature at 183GHz is shown in figure 13.

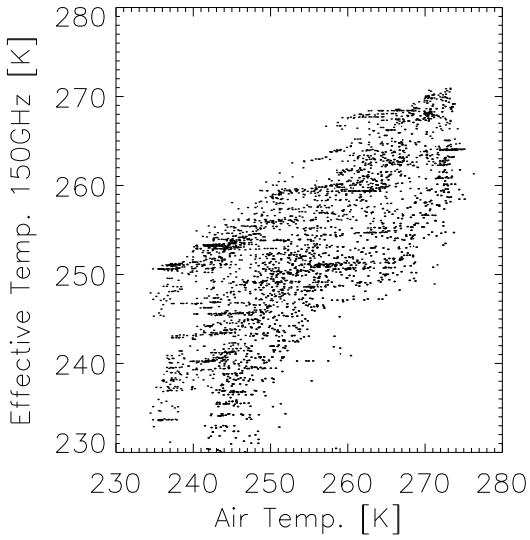

Figure 11 The Air temperature vs. the effective temperature at 150GHz. The correlation coefficient is 0.72.

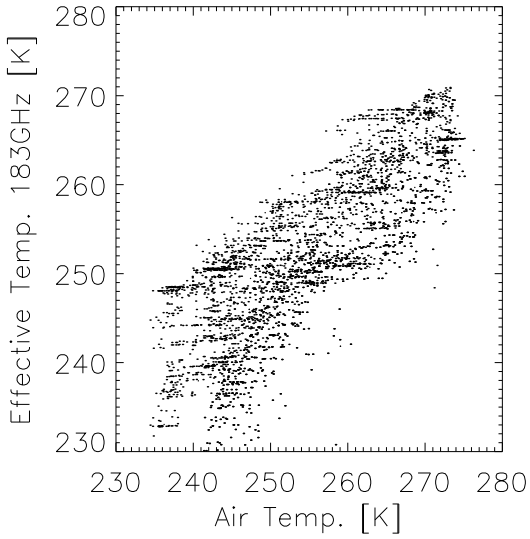

Figure 12 The Air temperature vs. the effective temperature at 183GHz. The correlation coefficient is 0.81.

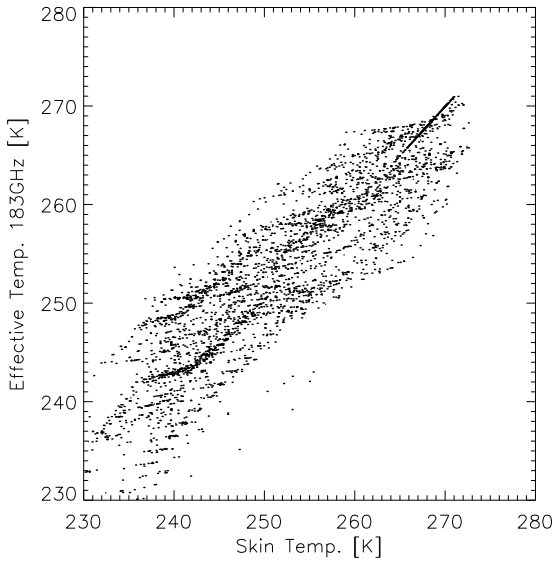

Figure 13 The skin temperature vs. the effective temperature at 183GHz. The correlation coefficient is 0.91.

High correlation coefficients at certain frequencies between on the one hand emissivity and effective temperature and on the other hand measurable quantities suggest that accurate estimates can be made in many cases. For the more complicated relationships both thermodynamic and microwave emissivity models are needed to translate measurements. Important input to the models can in some cases be found from measurements such as in figure 9.

MEAN SEASONAL MICROWAVE PARAMETERS

Figures 14 and 15 shows the mean seasonal microwave parameters for first-year ice and multiyear ice, respectively. L-band is different than all other channels and emissivity >89GHz is different than <89GHz.

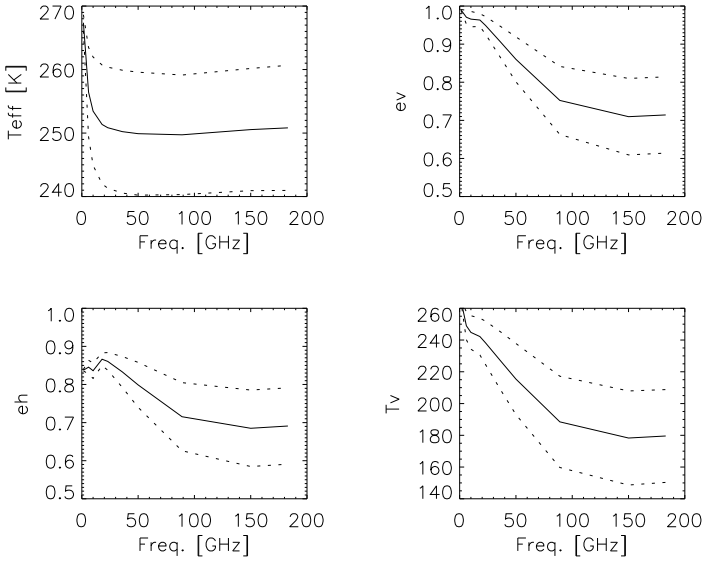

Figure 14 Mean seasonal first-year ice microwave parameters. +/- 1 STD is shown with dashed lines.

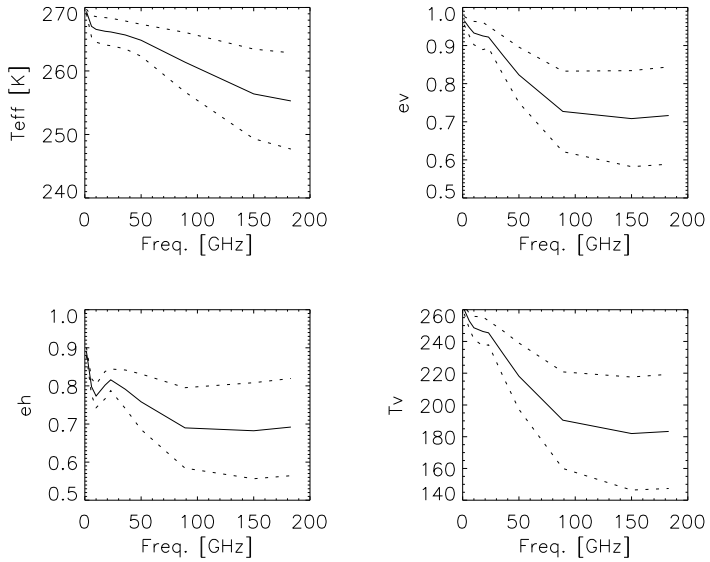

Figure 15 Mean seasonal multiyear ice microwave parameters. +/- 1 STD is shown with dashed lines.

DISCUSSION OF SEASONAL EMISSIVITY VARIATIONS

Applications such as assimilation of microwave data into numerical models suffer from the variable sea ice surface emissivity and effective temperature. Simple and clear relationships between on the one hand the microwave emissivity and effective temperature and parameterisable and measurable parameters on the other hand are not always found. Data quality check and selection is an inherent part of assimilation procedures in numerical models so that even 'noisy' relationships may be useful; even 5% of useful data points would be a success. Further, the IOMASA experiments by Schyberg and others show that simple parameterisations are feasible.

The complicated relationships where linear relationships are not readily found suggest that more sophisticated models could be useful for bringing data from measurement space into model space. Explicit modelling of surface emissivity even over sea ice is part of future systems.

The models functionality is demonstrated using seasonal snow and ice profile input from a thermodynamic model. The thermodynamic model output is expected to represent a wide range of natural situations in the Arctic Ocean. The model simulates emissivities within the limits of measurements reported in the literature (summarised in Tab. 1). Different relationships can be evaluated using the simulations. The seasonal variability is in general larger for frequencies >89GHz than lower frequencies. The variability is similar for the first and multiyear ice types and different for the two different snow covers. The latter is consistent with Eppler et al. (1992) noting that during winter, the level first-year ice thermal microwave signatures change primarily due to snow cover related processes.

REFERENCES

Eppler, D. T. and 14 others. Passive microwave signatures of sea ice. In: F. D. Carsey (Ed.). Microwave remote sensing of sea ice, geophysical monograph 68 (pp. 47-71). Washington DC: American Geophysical Union.

Haggerty, J. A. & J. A. Curry. Variability of sea ice emissivity estimated from airborne passive microwave measurements during FIRE SHEBA. Journal of Geophysical Research 106(D14),

15265-15277, 2001.
Hewison, T. J. & S. J. English. Airborne retrievals of snow and ice surface emissivity at millimeter wavelengths. IEEE Transactions on Geoscience and Remote Sensing 37(4), 1871-1879.
Mätzler, C., P.W. Rosenkranz, A. Battaglia and J.P. Wigneron, Eds., *Thermal Microwave Radiation - Applications for Remote Sensing, IEE Electromagnetic Waves Series*, London, UK, 2006.
Tonboe, R. A mass and thermodynamic model for sea ice. *Danish Meteorological Institute Scientific Report 05-10*, 2005.
Wiesmann, A. & C. Mätzler. Microwave emission model of layered snowpacks. *Remote Sensing of Environment 70*, 307-316, 1999.

APPENDIX

The correlation and covariance matrices for the 10 channels 1.4-183GHz are shown in tables A1-A2

Table A1. The correlation matrix for all 4 simulated profiles.

Teff	1,4	6	10	18	23	36	50	89	150	183
1,4	1	0,99	0,9835	0,9761	0,9737	0,9685	0,9593	0,8644	0,5394	0,4408
6	0,99	1	0,9987	0,9948	0,9931	0,989	0,9803	0,8882	0,5726	0,4761
10	0,9835	0,9987	1	0,9987	0,9977	0,9947	0,9873	0,9001	0,5922	0,4968
18	0,9761	0,9948	0,9987	1	0,9999	0,9984	0,9924	0,911	0,6108	0,5164
23	0,9737	0,9931	0,9977	0,9999	1	0,9991	0,9938	0,9149	0,6174	0,5232
36	0,9685	0,989	0,9947	0,9984	0,9991	1	0,9975	0,9301	0,644	0,5507
50	0,9593	0,9803	0,9873	0,9924	0,9938	0,9975	1	0,953	0,688	0,5966
89	0,8644	0,8882	0,9001	0,911	0,9149	0,9301	0,953	1	0,8617	0,7893
150	0,5394	0,5726	0,5922	0,6108	0,6174	0,644	0,688	0,8617	1	0,991
183	0,4408	0,4761	0,4968	0,5164	0,5232	0,5507	0,5966	0,7893	0,991	1
ev										
1,4	1	0,4348	0,4351	0,4229	0,2726	0,0906	0,008	-0,1386	-0,2091	-0,2121
6	0,4348	1	0,9369	0,6992	0,6244	0,3097	0,1602	-0,1642	-0,4401	-0,4958
10	0,4351	0,9369	1	0,8512	0,7801	0,5042	0,3635	0,0105	-0,3496	-0,4266
18	0,4229	0,6992	0,8512	1	0,9466	0,7946	0,6774	0,2741	-0,1834	-0,2703
23	0,2726	0,6244	0,7801	0,9466	1	0,9214	0,8336	0,4712	-0,0004	-0,0993
36	0,0906	0,3097	0,5042	0,7946	0,9214	1	0,9806	0,7427	0,3164	0,2192
50	0,008	0,1602	0,3635	0,6774	0,8336	0,9806	1	0,8542	0,4749	0,379
89	-0,1386	-0,1642	0,0105	0,2741	0,4712	0,7427	0,8542	1	0,842	0,7652
150	-0,2091	-0,4401	-0,3496	-0,1834	-0,0004	0,3164	0,4749	0,842	1	0,9885
183	-0,2121	-0,4958	-0,4266	-0,2703	-0,0993	0,2192	0,379	0,7652	0,9885	1
eh										
1,4	1	0,158	0,2242	0,2364	0,2187	0,1142	-0,0595	-0,4417	-0,5107	-0,5046
6	0,158	1	0,9193	0,802	0,854	0,7249	0,4642	-0,2641	-0,5771	-0,6043
10	0,2242	0,9193	1	0,9234	0,9363	0,8553	0,6344	-0,1254	-0,5469	-0,5969
18	0,2364	0,802	0,9234	1	0,9641	0,9121	0,7156	-0,0557	-0,5052	-0,5493
23	0,2187	0,854	0,9363	0,9641	1	0,9284	0,7043	-0,0696	-0,4878	-0,5288
36	0,1142	0,7249	0,8553	0,9121	0,9284	1	0,909	0,213	-0,3283	-0,3948
50	-0,0595	0,4642	0,6344	0,7156	0,7043	0,909	1	0,5667	-0,0156	-0,1048
89	-0,4417	-0,2641	-0,1254	-0,0557	-0,0696	0,213	0,5667	1	0,7723	0,6896
150	-0,5107	-0,5771	-0,5469	-0,5052	-0,4878	-0,3283	-0,0156	0,7723	1	0,9893
183	-0,5046	-0,6043	-0,5969	-0,5493	-0,5288	-0,3948	-0,1048	0,6896	0,9893	1
Tv										
1,4	1	-0,1081	-0,0792	-0,0767	-0,1665	-0,115	-0,0835	-0,1145	-0,157	-0,1601
6	-0,1081	1	0,9532	0,7963	0,8135	0,6431	0,5289	0,2945	0,0269	-0,04
10	-0,0792	0,9532	1	0,8935	0,8792	0,7529	0,659	0,4132	0,0848	0,0005
18	-0,0767	0,7963	0,8935	1	0,9709	0,9351	0,8725	0,6142	0,2351	0,1467
23	-0,1665	0,8135	0,8792	0,9709	1	0,9545	0,8905	0,6807	0,355	0,2731
36	-0,115	0,6431	0,7529	0,9351	0,9545	1	0,9842	0,8282	0,5069	0,4227
50	-0,0835	0,5289	0,659	0,8725	0,8905	0,9842	1	0,8997	0,6025	0,5184
89	-0,1145	0,2945	0,4132	0,6142	0,6807	0,8282	0,8997	1	0,8723	0,8064
150	-0,157	0,0269	0,0848	0,2351	0,355	0,5069	0,6025	0,8723	1	0,9901
183	-0,1601	-0,04	0,0005	0,1467	0,2731	0,4227	0,5184	0,8064	0,9901	1

Table A2. The covariance matrix for all 4 simulated profiles

Teff	1,4	6	10	18	23	36	50	89	150
1,4	1,8812	10,0882	12,2788	13,6166	13,8944	13,9845	13,6611	11,2983	6,6439
6	10,0882	55,1925	67,5354	75,1661	76,7632	77,3453	75,6187	62,8837	38,2028
10	12,2788	67,5354	82,86	92,4553	94,4866	95,321	93,3104	78,0842	48,4103
18	13,6166	75,1661	92,4553	103,4406	105,8003	106,8926	104,7964	88,3021	55,7892
23	13,8944	76,7632	94,4866	105,8003	108,2439	109,4241	107,3494	90,7125	57,6828
36	13,9845	77,3453	95,321	106,8926	109,4241	110,8213	109,0308	93,3107	60,8813
50	13,6611	75,6187	93,3104	104,7964	107,3494	109,0308	107,7998	94,2989	64,1509
89	11,2983	62,8837	78,0842	88,3021	90,7125	93,3107	94,2989	90,8228	73,7485
150	6,6439	38,2028	48,4103	55,7892	57,6828	60,8813	64,1509	73,7485	80,647
183	5,5103	32,2395	41,22	47,8722	49,6169	52,8437	56,4643	68,5636	81,1227
ev									
1,4	0,0002	0,0001	0,0002	0,0002	0,0001	0,0001	0	-0,0002	-0,0003
6	0,0001	0,0005	0,0007	0,0005	0,0004	0,0003	0,0003	-0,0004	-0,0012
10	0,0002	0,0007	0,0009	0,0009	0,0007	0,0007	0,0008	0	-0,0012
18	0,0002	0,0005	0,0009	0,0011	0,0009	0,0013	0,0016	0,0009	-0,0007
23	0,0001	0,0004	0,0007	0,0009	0,0008	0,0013	0,0017	0,0013	0
36	0,0001	0,0003	0,0007	0,0013	0,0013	0,0023	0,0033	0,0035	0,0017
50	0	0,0003	0,0008	0,0016	0,0017	0,0033	0,0047	0,0057	0,0037
89	-0,0002	-0,0004	0	0,0009	0,0013	0,0035	0,0057	0,0096	0,0094
150	-0,0003	-0,0012	-0,0012	-0,0007	0	0,0017	0,0037	0,0094	0,0128
183	-0,0003	-0,0013	-0,0015	-0,001	-0,0003	0,0012	0,003	0,0086	0,0128
eh									
1,4	0,0042	0,0007	0,0012	0,0009	0,0007	0,0004	-0,0002	-0,0018	-0,003
6	0,0007	0,0051	0,0054	0,0035	0,0032	0,0026	0,0017	-0,0012	-0,0038
10	0,0012	0,0054	0,0067	0,0046	0,004	0,0035	0,0026	-0,0007	-0,0041
18	0,0009	0,0035	0,0046	0,0036	0,0031	0,0027	0,0022	-0,0002	-0,0028
23	0,0007	0,0032	0,004	0,0031	0,0027	0,0024	0,0018	-0,0002	-0,0024
36	0,0004	0,0026	0,0035	0,0027	0,0024	0,0025	0,0023	0,0007	-0,0015
50	-0,0002	0,0017	0,0026	0,0022	0,0018	0,0023	0,0025	0,0018	-0,0001
89	-0,0018	-0,0012	-0,0007	-0,0002	-0,0002	0,0007	0,0018	0,0042	0,0046
150	-0,003	-0,0038	-0,0041	-0,0028	-0,0024	-0,0015	-0,0001	0,0046	0,0085
183	-0,0032	-0,0042	-0,0047	-0,0032	-0,0027	-0,0019	-0,0005	0,0043	0,0089
Tv									
1,4	8,8573	-2,3697	-2,1887	-2,4409	-5,8222	-5,6898	-5,3966	-10,0674	-15,251
6	-2,3697	54,2052	65,198	62,7196	70,3643	78,738	84,6033	64,0776	6,4514
10	-2,1887	65,198	86,3115	88,8008	95,9637	116,3192	133,0276	113,4542	25,6932
18	-2,4409	62,7196	88,8008	114,4355	122,0274	166,3554	202,8066	194,1759	82,0506
23	-5,8222	70,3643	95,9637	122,0274	138,0301	186,4886	227,3318	236,3637	136,1121
36	-5,6898	78,738	116,3192	166,3554	186,4886	276,5757	355,6477	407,0706	275,1137
50	-5,3966	84,6033	133,0276	202,8066	227,3318	355,6477	472,1053	577,7584	427,1573
89	-10,0674	64,0776	113,4542	194,1759	236,3637	407,0706	577,7584	873,4188	841,1959
150	-15,251	6,4514	25,6932	82,0506	136,1121	275,1137	427,1573	841,1959	1064,83
183	-15,5554	-9,619	0,1612	51,23	104,7376	229,4688	367,6662	777,9932	1054,611

Previous reports

Previous reports from the Danish Meteorological Institute can be found on:
http://www.dmi.dk/dmi/dmi-publikationer.htm